

FEDSM-ICNMM2010-' \$, (*

UNSTEADY AERODYNAMICS ON A LOW ASPECT RATIO FLAT PLATE

Adam Hart

Mechanical and Aerospace Engineering
University of Florida
Shalimar, FL, USA

Lawrence Ukeiley

Mechanical and Aerospace Engineering
University of Florida
Shalimar, FL, USA

ABSTRACT

The study of biological flight has shown the potential of using unsteady fluid mechanism to enhance lift and drag capabilities in low Reynolds number flight regimes. To help further the knowledge of unsteady aerodynamic fluid phenomena, a low aspect ratio flat plate is subjected to a pitching motion superimposed on a plunging motion. Variations in this motion are introduced by adding a phase lag to the pitching cycle relative to the plunge cycle. Particle Image Velocimetry (PIV) is used to measure the instantaneous velocity fields over the upper surface of the flat plate at several points in the motion cycle. These vector fields are then averaged over approximately 420 ensembles to obtain the mean velocity field at the points in the cycle. Three vortex detection algorithms are implemented to identify the center of the vortex structures created off the leading edge and track their convection downstream. Experiments show that phase lags between 75° and 90° are more prone to create organized vortex structures and convect them in close proximity to the upper surface of this low aspect ratio flat plate.

INTRODUCTION

The desire to design full functioning Micro Air Vehicles (MAV) is driving research in unsteady aerodynamics by both the biological and engineering communities due to the similarity in scale. The biological community has preformed many experiments investigating phenomena associated with flapping flight on a wide variety of insects and small wing animals [1] [2] [3] [4] [5] [6]. These experiments have demonstrated the importance of harnessing unsteady flow effects in order to operate in the low Reynolds number flight regimes. They conclude that unsteady vortical structures are important in the enhancement/destruction of lift and drag capabilities using mechanisms such as dynamic stall, rotational lift, and wake capture. Dynamic stall, also referred to as delayed stall, is induced from the creation of a large leading-edge vortex (LEV) located on the surface of the wing. Leading edge vortices have been shown to enhance lift well beyond the static angle of attack during dynamic stall [7]. The effect of this enhancement is determined by the stability of the LEV. Another

important benefit from the ability of small flapping flyers to change their lift and drag characteristics is that they become highly maneuverable.

Periodic pitching and plunging wings have been demonstrated to produce some of the same characteristics of small flyers [8]. The kinematic motions for plunging and pitching motion are defined respectively as

$$h(t) = (h_0 c) \cos(2\pi f t + \varphi_h), \quad (1.1)$$

$$\theta(t) = \theta_a \cos(2\pi f t + \varphi_\theta) + \theta_o. \quad (1.2)$$

The parameters φ_h and φ_θ in these equations allow for the creation of a phase lag between the pitching and plunging motions. The pitch-plunge kinematic motion is more realistic to what one might find in nature because natural fliers typically have a mechanism to alter their pitch while flapping their wings.

Various nondimensional parameters are useful in characterizing the kinematic motion of a pitching motion and the fluid properties. One important parameter is the reduced frequency and it is defined by the frequency of the plunge and pitch stroke (f), the chord (c), and the freestream velocity, shown below

$$k = \frac{\pi f c}{U_\infty}. \quad (1.3)$$

The reduced frequency provides a scaling between the airfoil and the desired kinematic motion being that it is a function of the chord and the frequency of the motion [9]. The Reynolds number provides insight into the fluid properties. The Reynolds number is defined by the freestream velocity, chord of the flat plate (c), and kinematic viscosity of the air (ν), resulting in

$$Re = \frac{U_\infty c}{\nu}. \quad (1.4)$$

Numerous experimental and numerical studies have been performed on two dimensional airfoils being subjected to

pitching, plunging, and pitching-plunging kinematic motions that are of the same nature of that being studied here (see for example [10] [11] [12] [13] [14]). Kang et al. [15] investigated the effects of Reynolds number on a pitching-plunging SD7003 airfoil and showed that larger LEVs occurred at lower Reynolds number. For a pure plunging SD7003, the same trend was shown. Bernal et al. [16] furthered this investigation by measuring unsteady forces on the pitching- plunging two dimensional SD7003 with a reduced frequency of 0.25 at a Reynolds number of 60,000. The pure plunge case showed to have an increase in the coefficient of lift, higher than predicted by unsteady linear theory. This is most likely created by the generation of the LEV. Therefore, unsteady effects of the LEV increase the lift by delaying dynamic stall.

Shyy et al. [17] completed numerical studies of the flow around a hawkmoth in hover. The vortex structures developed around the wing are found to be similar to low aspect ratio delta wings [18] [19]. Shyy et al. showed that the tip vortex enhances the stability of the LEV on the upper surface of the wing; therefore, the lift is also enhanced. The lift values past the critical point are enhanced by stabilizing the LEV and effectively delaying stall. It is this interaction between the LEV and the tip vortex that this study will try to understand in greater detail for future endeavors.

For this current effort, a flat plate with an aspect ratio of two will be used as the wing of interest. The low aspect ratio will allow for the investigation into tip vortices and their stabilizing role on the LEV. This wing will be driven through the pitching and plunging motions discussed above with an interest in varying the phase lag between the pitching and plunging cycles. Details of the velocity field in a streamwise plane at the three quarter span will be presented with specific application of three different vortex identification methods.

EXPERIMENTAL SETUP

All experiments for this effort were conducted in the University of Florida Research Engineering and Education Facility's (UF-REEF) low Reynolds number Aerodynamic Characterization Facility (ACF). The ACF is comprised of an open jet test section with a 42x42 inch square entrance to the test section. The test section is 15 feet long in the flow direction. Uniform flow is achieved in the test section to within 1% of the centerline velocity. The free stream turbulence intensity remains less than 0.11% for the desired free stream velocity of 4 m/s. Further characteristic information for the ACF can be found in Albertani et al [20].

A Dynamic Pitch-Plunge Rig, shown in Figure 1, was developed to perform the specific pitching and plunging motions used in this study. The sting is fixed to a rotational bearing at the front vertical rod and connected by unidirectional bearing at the back vertical rod. The two vertical rods are driven by two Parker ironless linear motors each connected to an Aries model AR-20AE driver providing the 787 mm of

linear travel. Controlling the motors is a Galil DMC-2020 motion controller. Labview software has been developed to communicate with the controller, giving it the ability to run prescribed motions and to enable the use of an onboard trigger signal. The controller will produce a standard TTL signal at a user defined motor position. This allows for a reliable trigger produced at the same phase in each cycle of the pitch-plunge motion.



Figure 1. Dynamic Pitch-Plunge Rig

With the objective to study unsteady aerodynamic phenomena, a LaVision Particle Image Velocimetry (PIV) system was used to make velocity field measurements around the flat plate at several specific times throughout the cyclical motion in a streamwise plane at $\frac{3}{4}$ span of the wing. This system consists of a Litron Nano L 135-15 laser which used to create a pair of 532nm pulses at 135 mJ/pulse which were expanded into a light sheet perpendicular to the flat plate along with an Imager ProX-4M camera comprised the PIV instrument system. The camera has a 2048x2048 pixel resolution CCD chip which is capable of acquiring images at 14 frames/sec and has 512 mb of onboard memory with external triggering capability. A Nikon 60mm lens with an f-number of 2.8 was used. These two systems were controlled through a system computer running DaVis software. The system computer was externally triggered from the TTL signal off the Galil controller. This signal initialized the Laser/Camera trigger sequence. A time delay of 500 μ s was assigned between the double frames of the camera which resulted in an approximately 19 pixel displacement in the free stream. The Imager ProX-4M camera was oriented to view a two dimensional cross section of the flat plate. An average resolution of 16.9pix/mm was achieved. The flow was seeded at the inlet to the wind tunnel using an Air Technologies Aerosol Generator TDA-4B Laskin nozzle seeder using olive oil. Based on the manufacturer specifications this is expected to produce particles approximately 1 μ m in diameter generated at a rate of 7x10¹⁰ particles per second. DaVis 7.2 PIV software from LaVision was used to analyze the PIV images with a multi-pass cross correlation algorithm. The first pass consisted of an interrogation region of 64x64 pixels with 50% overlap. Two more passes were conducted using a 32x32 pixel

interrogation window with 50% overlap. DaVis software finally post processes each single vector field and removes vectors which are greater than 2.5 times the root mean squared (rms) value of its neighbors. This procedure is completed for 420 double frame images at a single phase in the motion. The mean velocity field was calculated by averaging each of the 420 velocity fields. Any velocity vector that resulted in a deviation outside of two standard deviations throughout the ensemble was also removed. This process typically eliminated 12% of the vectors at any given location.

EXPERIMENTAL PARAMETERS

For this particular study, four different pitch-plunge kinematic motions will be investigated. The variation in these motions will be incurred from a changing of the phase lag between the pitch and plunge motions given by Equations 1.1 and 1.2. To maintain a Reynolds number of 40,000, a reduced frequency (k) of 0.25 and freestream velocity (U_∞) of 4 m/s, a frequency (f) of 2.02 Hz will be used for each case. The normalized plunge amplitude (h_0) is 0.5 for all cases, resulting in a full plunge distance of 1 chord length. All cases are rotated about the quarter chord of the flat plate. Cases 1, 3, and 4 are variations of a pitch-plunge kinematic motion. Each case has pitch amplitude (θ_0) equal to 8.00° with a constant pitch (θ_a) of 8.45° . A variation in phase lags of 90° , 75° , and 30° are used in these cases respectively. A phase lag of 90° is representative of a hovering kinematic motion. A phase lag of 75° should be similar to the 90° phase lag with minute differences. The 30° phase lag on the other hand should provide large changes in the flow structures created off the leading edge. In contrast to these three motions, Case 2 is a pure plunge motion. The pitch is fixed at 8.00° . All case parameters have been summarized in Table 1. Figure 2 presents a graphical representation of each case for 1 cycle. PIV mean flow measurements have been made at normalized times of 0, 0.25, 0.50, and 0.75 for all cases. Cases 1 and 3 have additional velocity field measurements acquired at times 0.33 and 0.42.

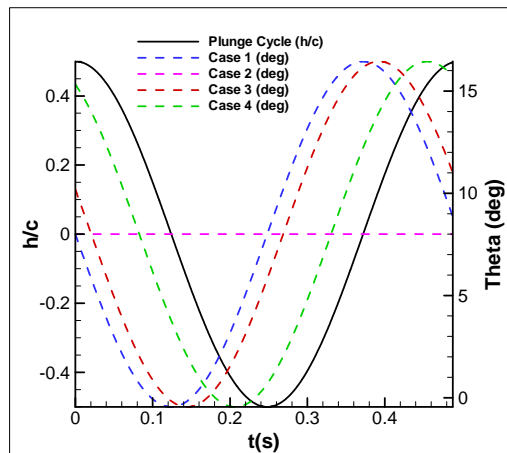


Figure 2. Pitch Plunge cases for 1 cycle

Table 1. Case Parameters

	Case 1	Case 2	Case 3	Case 4
h_0	0.5	0.5	0.5	0.5
θ_0 [°]	8.00	0.00	8.00	0.00
θ_a [°]	8.45	8.45	8.45	8.45
f [Hz]	2.02	2.02	2.02	2.02
ϕ_n [°]	0	0	0	0
ϕ_θ [°]	90	-	75	30
ϕ_{lag} [°]	90	-	75	30
k	0.25	0.25	0.25	0.25

VORTEX IDENTIFICATION TECHNIQUES

Vortex structures created off the leading edge of the flat plate have been shown to enhance the aerodynamic performance as they convect downstream. In order to understand the interaction between these structures in the flow, one must first identify the location of LEVs and track their convection downstream. Three methods of detection are investigated in this experiment: Line Integral Convolution Streamlines, Γ_1 vortex core detection, and VortFind. These three methods were selected based on their relative ease to implement and their ability to be used on PIV data.

The simplest form of detecting vortex cores in a flow field is by plotting the streamlines. This can be inherently difficult due to the tediousness of selecting the appropriate stream line corresponding to the given vortex core. Stalling et al [21] utilized the Line Integral Convolution (LIC) technique for generating steam line images from vector field data such that the total number of stream lines plotted is minimized. Utilizing the LIC technique, the capability for a visual representation of fluid structures located around the flat plate is achieved. This method is limited by its lack of ability to calculate and quantify the probability of vortex cores.

Graftieaux et al [22] [23] and Morse et al [24] used a technique based on circulation to identify the center location of vortices in unsteady turbulent flow. Their experiments resulted in a robust detection algorithm based on the scalar Γ_1 to identify the centers of any vortices within the flow respectively. These scalars are defined as

$$\Gamma_1(P) = \frac{1}{N} \sum_S \frac{(\overline{PM} \times \overline{U_M}) \cdot z}{\|\overline{PM}\| \cdot \|\overline{U_M}\|} dS, \quad (1.5)$$

The interrogation area (S) is defined by a block of discrete points around a point of interest (P). A summation is completed through all the points around P with M being the current point of interest. The Γ_1 criteria is effectively the average of the difference in angle between the PM and U_M vectors for all points included in the interrogation area around P . If the average of differences of the angles between the PM and U_M vectors is equal to 90° for the interrogation region, Γ_1 equals 1 or -1 for counter clock-wise and clock-wise rotation

respectively. Vortex centers are typically located where the magnitude of Γ_1 reaches values ranging from 0.9 to 1.

Pemberton et al [25] used what they termed a VortFind algorithm to find vortical structures in a 2D velocity field. In this method each vector is assigned its corresponding angle (α) with respect to the horizontal. A value of β is then assigned to each location in the vector field corresponding to Table 2.

Table 2. Relationship between α and β values

$0^\circ \leq \alpha < 120^\circ$	$\beta = 0$
$120^\circ \leq \alpha < 240^\circ$	$\beta = 1$
$240^\circ \leq \alpha < 360^\circ$	$\beta = 2$

An iterative process is then performed over each point on the 2D vector field for the two nearest points with differing beta values of $\beta = 0, 1$ and 2 . The value $p, q,$ and r are assigned the distance to each beta value respectively. Note that one of $p, q,$ or r will be zero due to the current locations beta value. A final minimum value (l) is assigned to the current point, given by the following relationship

$$l = p^2 + q^2 + r^2. \quad (1.6)$$

Scaling the values by

$$l_{new} = \exp\left\{-\frac{l_{max}}{l_{min}} l\right\}, \quad (1.7)$$

where l_{max} and l_{min} are the corresponding maximum and minimum values of l , changes the vortex cores to maximums and helps discern the surrounding flow and vortex flow. Pemberton showed this method to prove useful for an approximation of the vortex cores location, rather than an exact method.

This paper will utilize all these techniques to identify vortex structures within the flow around the flat plate. The overall objective is to understand how these structures augment lift and drag. Locating the vortices and quantifying the strength of these structures is an important first step.

VELOCITY MEASUREMENTS

Table 3 shows the phase averaged streamwise component of velocity normalized by the mean flow for all cases. Looking at Case 1 during the downstroke from time 0.25 to 0.50, a region of separated flow appears on the upstream portion of the plate and grows as the flat plate continues along the downstroke. The pitch of the flat plate goes from nominally 8° to -0.42° and then back to 8° throughout the downward plunge to the bottom of the stroke. The separated flow region is largest between -0.42° and approximately 5° pitch which corresponds to times 0.25 and 0.42 respectively. During this duration of the cycle, the plunge velocity is at its maximum, leading to a high effective angle of attack.

Case 3, corresponding to a phase lag of 75° , is remarkably similar to Case 1 as one might expect. One notable difference is that during the downstroke the separation over the top of the flat plate is not as pronounced as it is in Case 1.

Case 2 demonstrates a large separation on the top of the flat plate for the downstroke. This separation differs from Cases 1 and 3 because it is larger and remains large throughout the entire downstroke. Cases 1 and 3 showed a gradual increase and decrease in size of the separation, which after comparing with Case 2, is most likely caused by the rotation rate of the flat plate.

Case 4 has a phase lag of 30 degrees which lies in between the larger phase lags (Cases 1 and 3) and the pure plunge (Case 2). The first notable difference is a region of separation already existing over the flat plate at time 0.00. The separation grows during the first half of the downstroke with limited vortex creation. At the bottom of the downstroke, the large separation is convected downstream of the flat plate.

It is interesting to contrast the results for the low aspect ratio flat being used here to the case of a semi infinite span flat plate. Rausch et al. [26] completed studies similar to that of Case 1 with the exception of an infinite span flat plate. The vortex roll up in the two dimensional case is much larger and lifted further off the surface of the flat plate than that of the low aspect ratio flat plate. At times 0.31 thru 0.50, the reattachment of the flow over the upper surface reattaches at the backend of the plate. The three dimensional case shows the flow reattaches mid chord of the wing. It can be concluded that the mass flux induced from the tip vortices play a dominant part in suppressing the LEV onto the surface of the wing.

Table 4, Table 5, Table 6, and Table 7 show the results for each vortex detection schemes along with streamlines using the LIC technique. There is strong agreement when comparing the streamline plots with the Γ_1 vortex identification. Due to the nature of the Γ_1 scheme, one would expect to see higher probability of vortex cores where the streamlines make large angled turns. For instance, Case 1 at time 0.50, the streamline plot shows two locations where the streamlines form circular paths. The Γ_1 detection scheme also agrees that these locations have a large probability for vortex structure cores. In contrast, the VortFIND scheme tends to have less agreement with the previous schemes in terms of the location of vortices. An example is Case 1 at time 0.50. Four potential cores are detected. The problem associated with this technique is defining a threshold value. If one were to select the two highest detected values at time 0.50, the two vortex cores seen by the previous methods are identified. However, when comparing the locations detected between the Γ_1 and the stronger VortFIND cores, good agreement is achieved.

Table 4 shows the results of the three vortex detection schemes for Case 1. The evolution of vortices created in the shear layer

that originates off the LE using the Γ_1 vortex identification techniques is clearly visible here. At time 0.00 there is no evidence of vortices throughout the flow. The middle of the downward plunge stroke shows that one vortex has separated from the LE of the plate. As the plate begins to plunge at a slower rate to the bottom of cycle, more distinct vortices appear to form and are shed aft of the plate. Finally, at time 0.50, two vortices are being convected in close proximity to the upper surface of the flat plate. Case 3, shown in Table 5, results in a similar trend.

Case 2, presented in Table 6, results in minimal production of a strong discrete vortex core throughout the downward stroke. At time 0.25, the Γ_1 criterion shows low probability of a defined vortex structure forming off the LE. At the bottom of the plunge cycle, defined structures are not seen.

Case 4 shows the existence of a strong vortex core sitting in close proximity to the upper surface of the flat plate at approximately 30% of the chord length at time 0.00 in Table 7. Throughout the downward plunge, the development of strong vortex cores is not seen.

SUMMARY

PIV experimental data has been used to determine the mean velocity fields over a low aspect ratio flat being subjected to a pitch plunge kinematic motion. Varying the phase lag between the plunging and pitching motion resulted in the creation of different flow structures over the flat plate. Case 1 (pitching cycle lagging the plunging cycle by 90°) produced the most organized vortex structures closest to the upper surface of the wing. Case 3 (pitching cycle lagging the plunging cycle by 75°) resembled that of Case 1 but vortices created were more disorganized with their corresponding cores located farther from the surface of the wing. Presumably, this would result in a decrease in lift characteristics. It is shown that phase lags between 75° and 90° enhance the flows ability to develop strong vortex structures off the LE. These structures convect down stream in relatively close approximation to the upper surface of the wing, presumably enhancing lift through the use of unsteady fluid mechanisms.

ACKNOWLEDGMENTS

The work has been supported by Air Force Office of Scientific Research's Multidisciplinary University Research Initiative (MURI) and the Florida Center for Advancement Aero-Propulsion (FCAAP). Also, we would like to personally thank Roland Scheffer and Capt. Judd Babcock of the Air Force Research Lab and Erik Sällström of UF.

REFERENCES

[1] R. Dudley, "Biomechanics of Flight in Neotropical Butterflies: Aerodynamics and Mechanical Power Requirements," *Journal of Experimental Biology*, pp. 335-

357, 1991.

[2] C. P. Ellington, "The Novel Aerodynamics of Insect Flight: Applications to Micro-Air Vehicles," *The Journal of Experimental Biology* 202, pp. 3439-3448, 1999.

[3] S. P. Sane and M. H. Dickinson, "The Control of Flight Force by a Flapping Wing: Lift and Drag Production," *The Journal of Experimental Biology*, pp. 2607-2626, 2001.

[4] S. Vogel, "Flight in *Drosophila* 1. Flight Performance of Tethered Flies," *Journal of Experimental Biology*, pp. 567-578, 1966.

[5] S. Vogel, "Flight in *Drosophila* 2. Variations in Stroke Parameters and Wing Contour," *Journal of Experimental Biology*, pp. 383-392, 1967.

[6] A. P. Willmott and C. P. Ellington, "The Mechanics of Flight in the Hawkmoth *Madruca sexta*," *Journal of Experimental Biology*, pp. 2705-2722, 1997.

[7] M. H. Dickinson, "The Effects of Wing Rotation on Unsteady Aerodynamic Performance at Low Reynolds Numbers," *Journal of Experimental Biology*, pp. 179-206, 1994.

[8] M. F. Platzer, K. D. Jones, J. Young, and J. S. Lai, "Flapping-Wing Aerodynamics: Progress and Challenges," *AIAA Journal*, vol. 46, pp. 2136-2149, Sep. 2008.

[9] M. S. Triantafyllou, A. H. Techet, and F. S. Hover, "Review of Experimental Work in Biometric Foils," *Journal of Oceanic Engineering*, vol. 29, pp. 585-594, Jul. 2004.

[10] Y. S. Baik, J. M. Rausch, L. P. Bernal, and M. V. Ol, "Experimental Investigation of Pitching and Plunging Airfoils at Reynolds Number between $1e4$ and $6e4$," in *AIAA 2009-4030*, San Antonio, 2009.

[11] S. Sunada and A. Sakaguchi, "Unsteady Forces on a Two-dimensional Wing in Plunging and Pitching Motions," *AIAA Journal*, pp. 1230-1239, 2001.

[12] D. Rival and C. Tropeo, "Characteristics of a Pitching and Plunging Airfoils Under Dynamic-Stall Conditions," *Journal of Aircraft*, vol. 47, pp. 80-86, Jan. 2010.

[13] J. Rausch and A. Altman, "Vortex Formation of Plunging Flat Plates," in *AIAA Aerospace Sciences Meeting*, Orlando, 2009.

[14] J. Young and J. C. S. Lai, "Vortex Lock-In Phenomenon in the Wake of a Plunging Airfoil," *AIAA Journal*, vol. 42, no. 2, pp. 485-490, Feb. 2007.

[15] C.-k. Kang, Y. S. Baik, L. Bernal, M. V. Ol, and W. Shyy, "Fluid Dynamics of Pitching and Plunging Airfoils of Reynolds Number between 1×10^4 and 6×10^6 ," *AIAA 2009-536*, Jan. 2009.

[16] L. P. Bernal, M. V. Ol, D. P. Szczublewski, and C. A. Cox, "Unsteady Force Measurements in Pitching-Plunging Airfoils," *AIAA 2009-4031*, Jan. 2009.

[17] W. Shyy and H. Liu, "Flapping Wings and Aerodynamic

Lift: The role of Leading-Edge Vortices," *AIAA Journal*, vol. 45, no. 12, pp. 2817-2819, Dec. 2007.

- [18] C. Van Den Berg and C. P. Ellington, "The Vortex Wake of a 'hovering' model hawkmoth," *Royal Society of London Philosophical Transactions Series B*, pp. 317-328, Mar. 1997.
- [19] C. P. Ellington, C. Van Den Berg, A. P. Willmott, and A. L. R. Thomar, "Leading-edge vortices in insect flight," *nat*, vol. 384, pp. 626-630, Dec. 1996.
- [20] R. Albertani, et al., "Validation of a Low Reynold Number Aerodynamic Characterization Facility," in *AIAA Paper 2009-0880*, Orlando, Jan. 2009.
- [21] D. Stalling and H. Hans-Christian, "Fast and Resolution Independent Line Integral Convolution," 1995.
- [22] L. Graftieaux, M. Michard, and N. Grosjean, "Combining PIV,POD, and Vortex Identification Algorithms for the study of Unsteady Turbulent Swirling Flows," *Measurement Science and Technology*, vol. 12, pp. 1422-1429, Aug. 2001.
- [23] J. C. Bera, M. Michard, N. Grosjean, and G. Comte-Bellot, "Flow Analysis of Two-Dimensional Pulsed Jets by Particle Image Velocimetry," *Experiments in Fluids* , pp. 519-532, Jan. 2001.
- [24] D. R. Morse and J. A. Liburdy, "Vortex Dynamics and Shedding of a Low Aspect Ratio, Flat Wing, at Low Reynolds Numbers and High Angles of Attack ," *Journal of Engineering Fluids*, vol. 131, May 2009.
- [25] R. J. Pemberton, S. R. Turnock, T. J. Dodd, and E. Rogers, "A Novel Method for Udentifying Vortical Structures," *Journal of Fluids Structures*, vol. 16, no. 8, pp. 1051-1057, Oct. 2002.

ANNEX A

Table 3. Normalized U component of velocity $\left(\frac{U}{U_\infty}\right)$ at $\frac{3}{4}$ span

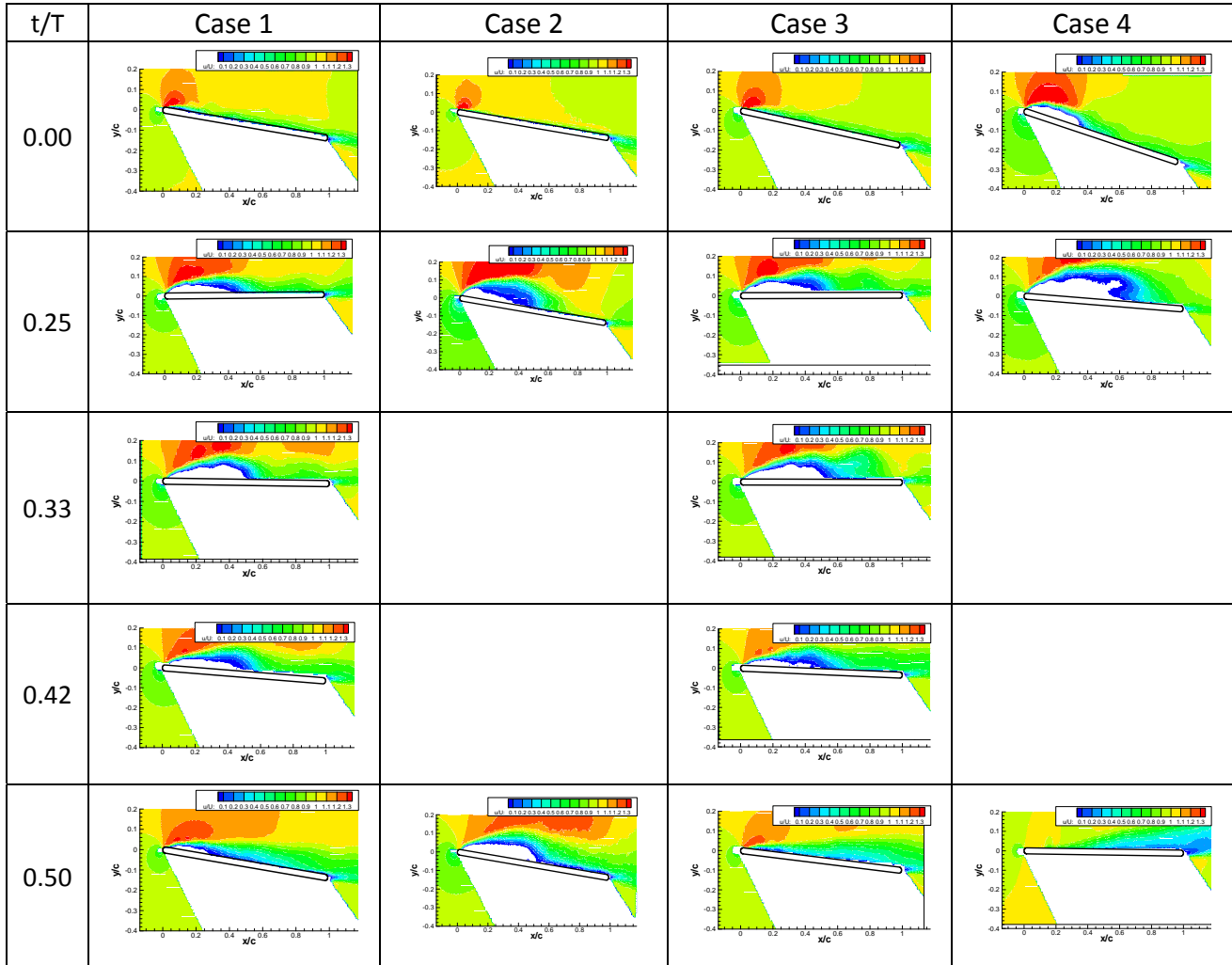


Table 4. Vortex Identification Scheme results for Case 1

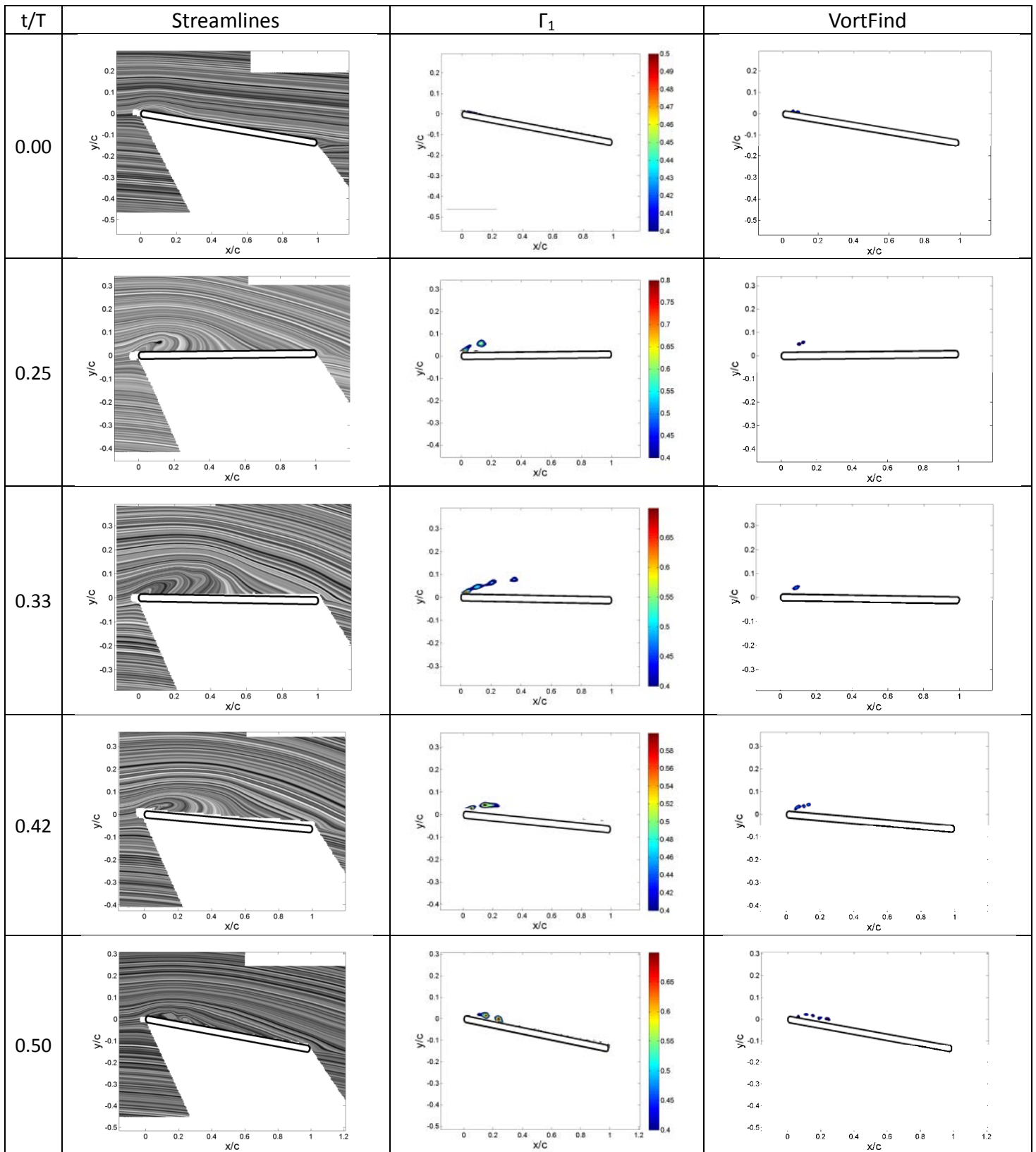


Table 5. Vortex Identification Scheme results for Case 3

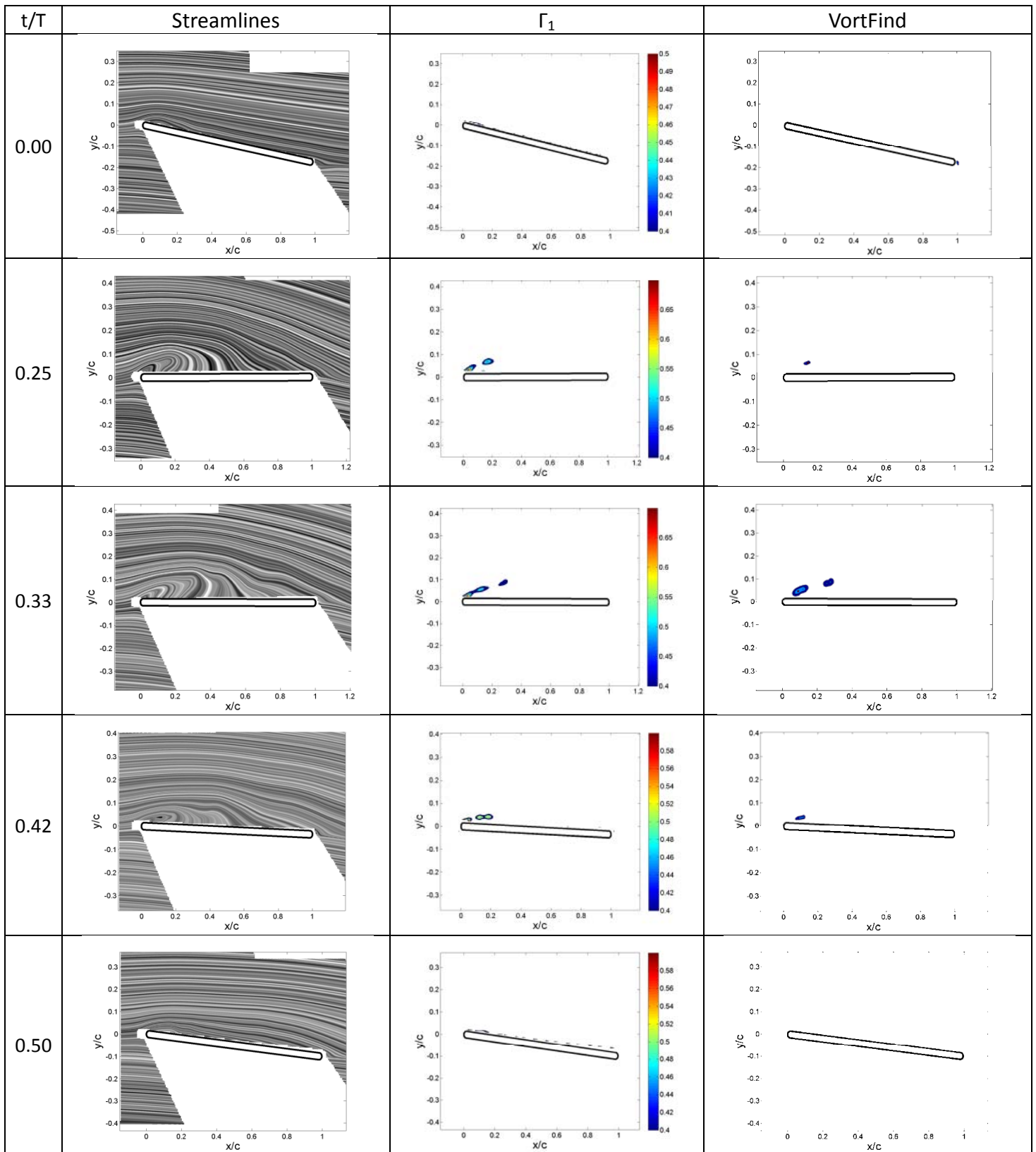


Table 6. Vortex Identification Scheme results for Case 2

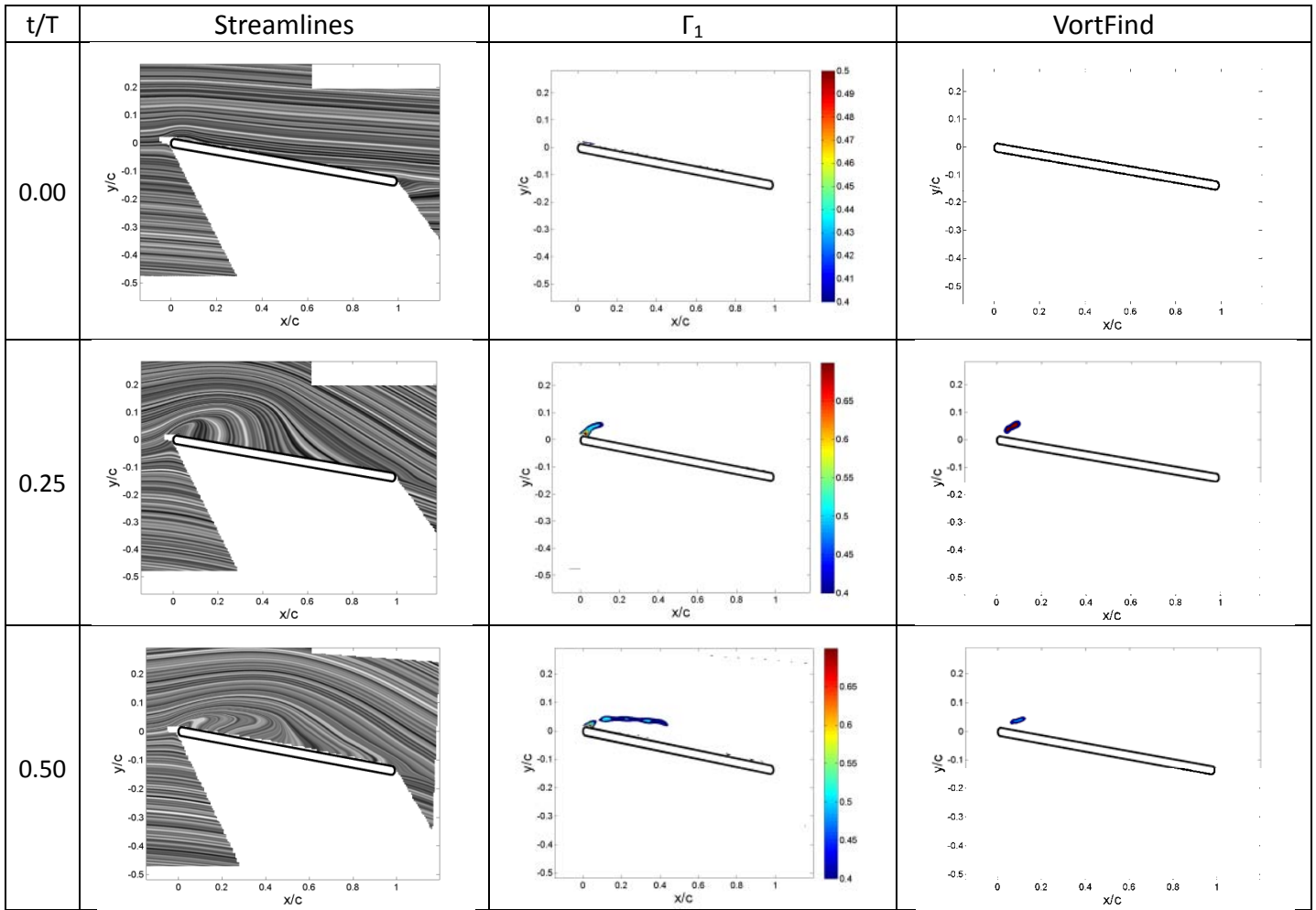


Table 7. Vortex Identification Scheme results for Case 4

